SCIENTIFIC REPORTS

OPEN

SUBJECT AREAS:
CHEMICAL ENGINEERING
COMPUTATIONAL SCIENCE

Received
21 March 2014

Accepted
4 August 2014

Published
2 September 2014

Correspondence and requests for materials should be addressed to E.J.R.P. (eric.parteli@fau.de)

Attractive particle interaction forces and packing density of fine glass powders

Eric J. R. Parteli[1], Jochen Schmidt[2], Christina Blümel[2], Karl-Ernst Wirth[2], Wolfgang Peukert[2] & Thorsten Pöschel[1]

[1]Friedrich-Alexander-Universität Erlangen-Nürnberg, Germany, [2]Institute of Particle Technology (LFG), University of Erlangen-Nuremberg (FAU), Cauerstraße 4, D-91058 Erlangen, Germany.

We study the packing of fine glass powders of mean particle diameter in the range (4–52) μm both experimentally and by numerical DEM simulations. We obtain quantitative agreement between the experimental and numerical results, if both types of attractive forces of particle interaction, adhesion and non-bonded van der Waals forces are taken into account. Our results suggest that considering only viscoelastic and adhesive forces in DEM simulations may lead to incorrect numerical predictions of the behavior of fine powders. Based on the results from simulations and experiments, we propose a mathematical expression to estimate the packing fraction of fine polydisperse powders as a function of the average particle size.

The packing behavior of powders can be strongly influenced by inter-particle attractive forces of different types, such as adhesion and non-bonded van der Waals forces[1–6]. The relevance of the different types of attractive interactions for the packing density of powders of different materials and particle size distributions is, however, largely uncertain. That is, it is a challenging problem to *predict* the packing density of a certain granular system specified by the particle size distribution and the material properties of the particles[7,8].

Numerical simulations by means of the Discrete Element Method (DEM)[9,10] can offer a helpful tool in the investigation of the packing behavior of powders. In this type of numerical simulations, Newton's equation of motion is solved for all particles simultaneously by taking into account the forces and torques acting on each particle, both due to external fields and due to interactions with other particles in the system. However, in order to make reliable predictions of the behavior of the bulk from DEM simulations, an accurate physical modeling of the relevant forces governing the interactions between the particles is required.

Most previous studies of density of dry powder packings using DEM simulations were focused on monodisperse systems and included either van der Waals interactions[7,11,12] or adhesive forces during contact[13,14]. Indeed, typical powders are poorly sorted and may contain a broad interval of particle sizes. For fine powders, the attractive interactions between particles of different sizes should have an important effect on the dynamics, since cohesive forces become increasingly relevant compared to gravitational forces as the particle size decreases[4]. Therefore, particle size distribution plays an essential role not only due to geometrical constraints[15–20] but also because attractive forces have different influence for particles of different size. Consequently, the size distribution of particles and the adequate description of attractive forces acting on particles of different size should be taken into account in DEM simulations in order to yield a predictive description of fine powders.

The aim of our work is to provide numerical evidence that DEM simulations are able to describe the packing of fine powders correctly, that is in quantitative agreement with experiments, provided both the particle size distribution and the adequate model of attractive particle interaction are taken into account. We will show that this model should contain both relevant contributions due to adhesion (here modeled through JKR theory[21]) and van der Waals interactions. Neglecting any of these contributions leads for the case of fine powders to unacceptable deviations, that is the DEM method renders unreliable. We believe that this result, obtained for the packing of fine glass powders will be of relevance also for other systems, in particular, when the system contains a significant fraction of small particles or a wide distribution of particle sizes.

We characterize the particle size distribution by means of $q_3(d) \equiv \mathrm{d}Q_3(d)/\mathrm{d}d$ where $Q_3(d)$ is the fraction of mass of all particles of diameter d or smaller, relating to the probability density of particle diameters, $p(d)$, via

$$q_3(d) = \frac{d^2 p(d)}{\int_0^\infty p(d')\ (d')^2 \mathrm{d}d'}. \qquad (1)$$

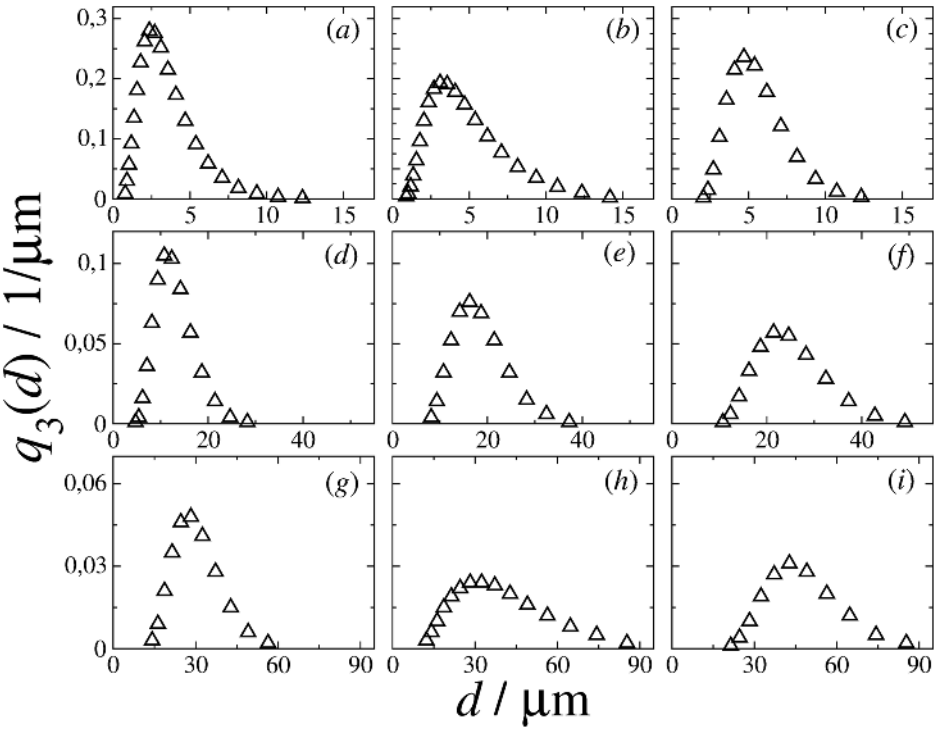

Figure 1 | Experimental particle size distributions. The figure shows the volume density distributions q_3 (see Eq. (1)) of the samples *a–i* used in the experiments. Each plot gives the volume density distribution $q_3(d)$ as a function of the particle diameter d in the sample.

Figure 1 shows the size distribution, $q_3(d)$, of our experimental samples, each of them averaged over 5 independent measurements. For each sample, Tab. I provides the mean diameter, $\langle d\rangle \equiv \int_0^\infty q_3(d)d\mathrm{d}d$, and the obtained packing fraction, φ, again averaged over 5 independent measurements. Further, the corresponding 1%, 50%, and 99% quantiles, $d_{1,3}$, $d_{50,3}$, and $d_{99,3}$, respectively, are given defined as $d_{x,3} \equiv Q_3^{-1}(x/100)$, where Q_3^{-1} is the inverse of $Q_3(d)$. The values from Tab. I are used furtheron for reference in the subsequent figures.

We simulate the process using DEM, that is, simultaneously solving Newton's equations of translational and rotational motion for all particles. There is a variety of models to describe the contact forces in DEM simulation, suitable for different particle geometry and material behavior, for an overview see, e.g.[10,22–24]. In the present paper, we assume viscoelastic interaction in normal direction[25] and apply a modified Cundall-Strack model[9] for the tangential direction[26]. The corresponding forces read

Table I | Summary of the powder characteristics of samples *a–i*: Quantities $d_{1,3}$, $d_{50,3}$ and $d_{99,3}$; mean particle size $\langle d\rangle$, and obtained packing fraction φ. Samples *a–i* correspond to the subplots of Fig. 1

sample	$d_{1,3}/\mu m$	$d_{50,3}/\mu m$	$d_{99,3}/\mu m$	$\langle d\rangle/\mu m$	φ
a	1.05	3.22	9.51	3.88	0.20
b	1.40	4.47	12.33	5.36	0.19
c	2.65	5.35	10.79	6.03	0.29
d	6.31	12.49	23.89	13.96	0.40
e	9.18	17.81	33.44	19.87	0.47
f	2.87	24.47	44.94	27.21	0.51
g	15.78	29.56	53.74	32.83	0.52
h	14.15	38.37	89.13	44.38	0.51
i	25.27	46.85	85.05	52.04	0.54

$$\vec{F}_n = \min\left(0, -\rho\xi^{3/2} - \frac{3}{2}A_n\rho\sqrt{\xi}\dot{\xi}\right)\vec{e}_n, \tag{2}$$

where

$$\xi = R_1 + R_2 - |\vec{r}_1 - \vec{r}_2| \tag{3}$$

is the compression of particles of radii R_1 and R_2 at positions $\vec{r}_1$ and $\vec{r}_2$, and $\vec{e}_n \equiv (\vec{r}_1 - \vec{r}_2)/|\vec{r}_1 - \vec{r}_2|$ is the normal unit vector. The elastic parameter of Eq. (2), ρ, is a function of the Young's modulus, Y, the Poisson's ratio ν, and the effective radius $R_{\mathrm{eff}} \equiv R_1R_2/(R_1 + R_2)$,

$$\rho \equiv \frac{2Y}{3(1-\nu^2)}\sqrt{R_{\mathrm{eff}}}, \tag{4}$$

and the dissipative parameter, A_n, depends, moreover, on the material viscosities. For details see[25]. While ρ can be computed directly from material characteristics which are easily available for a variety of materials, the viscosities needed for A_n are not directly available. To determine A_n, therefore, we use a relation between the coefficient of restitution, ε, for the collision of two isolated particles and A_n[27–29] where the Padé approximation from[30] was employed.

The tangential force reads[26]

$$\vec{F}_t = -\min\left[\mu|\vec{F}_n|, \int_{\mathrm{path}} \frac{4G}{2-\nu}\sqrt{R_{\mathrm{eff}}\xi}\mathrm{d}s + A_t\sqrt{R_{\mathrm{eff}}\xi}v_t\right]\vec{e}_t, \tag{5}$$

where μ is the Coulomb friction coefficient and G is the shear modulus, which is given by the equation, $2G = Y/(1 + \nu)$. The integral in Eq. (5) is performed over the displacement of the particles at the point of contact for the duration of the contact[9] and $\vec{v}_t = v_t\vec{e}_t$ stands for the relative tangential velocity at the point of contact, where $\vec{e}_t$ is the corresponding unit vector. The tangential dissipative parameter, A_t, characterizes the surface roughness and is chosen such that the prefactors of the normal and tangential deformation rates ($\dot{\xi}$ and v_t) in Eqs. (2) and (5), respectively, are of the same order of magnitude[31]. Using this assumption, Ref. [32] found excellent agreement between simulation results and experimental values of particle velocity pro-

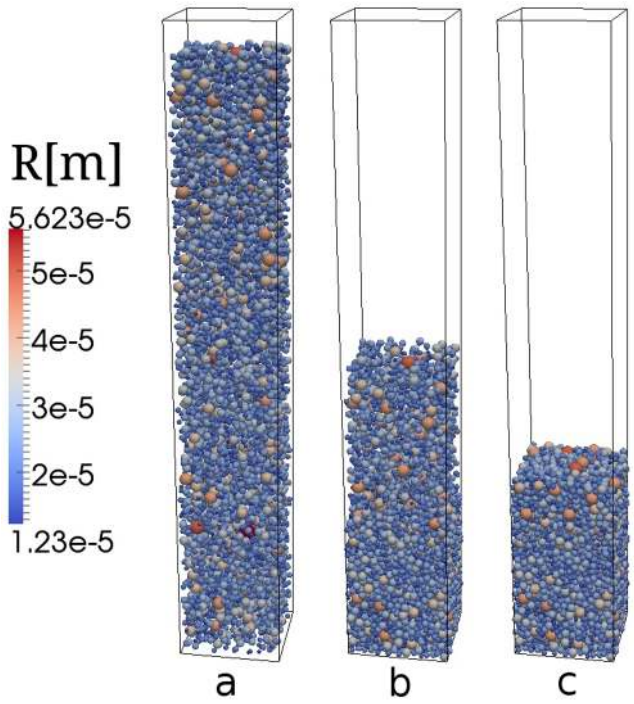

Figure 2 | Numerical simulation of the powder packing. The figure displays a packing of 6172 cohesionless spherical particles of size distribution shown in Fig. 1i. The box size is $L_x = L_y = 0.3351$ mm (periodic boundary conditions) and $L_z = 4.2$ mm. Figures a–c show snapshots at time (in milliseconds) 0, 20 and 140.

files in a gravity-driven shearing experiment. By comparing Eqs. (2) and (5), we obtain $A_t \approx A_n Y/(1-\nu^2)$.

Adhesion is taken into account via the JKR model[14,21,33,34]

$$\vec{F}_{\mathrm{JKR}} = 4\sqrt{\frac{\pi a^3 \gamma Y}{2(1-\nu^2)}}\vec{e}_{\mathrm{n}}, \tag{6}$$

where a is the contact radius, related to the deformation ξ through

$$\xi = a^2/R_{\mathrm{eff}} - \sqrt{8(1-\nu^2)\pi a\gamma/Y}, \tag{7}$$

and γ is the surface energy density, which is a characteristic of the particle material[35].

To compute the force, $\vec{F}_{\mathrm{JKR}}$, through Eq. (6), the contact radius, $a(\xi)$ is determined from Eq. (7) as a function of the deformation ξ. Thus, Eq. (7) can be rewritten in the form[14]

$$a^4 - [2R_{\mathrm{eff}}\xi]a^2 - \left[8\left(1-\nu^2\right)\pi\gamma R_{\mathrm{eff}}^2/Y\right]a + \left[R_{\mathrm{eff}}^2\xi^2\right] = 0. \tag{8}$$

This equation can be solved analytically to obtain the contact radius, a, see Eq. (18).

For the case of fine powders, van der Waals force may have a non-negligible influence on the dynamics of the system. It is given by[36,37]

$$\vec{F}_{\mathrm{vdW}} = \begin{cases} \dfrac{A_H R_{\mathrm{eff}}}{6D_{\mathrm{min}}^2}\vec{e}_n & \text{if} \quad \xi > 0, \\ \dfrac{A_H R_{\mathrm{eff}}}{6(\xi - D_{\mathrm{min}})^2}\vec{e}_n & \text{if} \quad -D_{\mathrm{max}} \le \xi \le 0 \\ 0, & \text{if} \quad \xi < -D_{\mathrm{max}}, \end{cases} \tag{9}$$

where ξ is given by Eq. (3). The Hamaker constant is related to the surface energy density via[2]

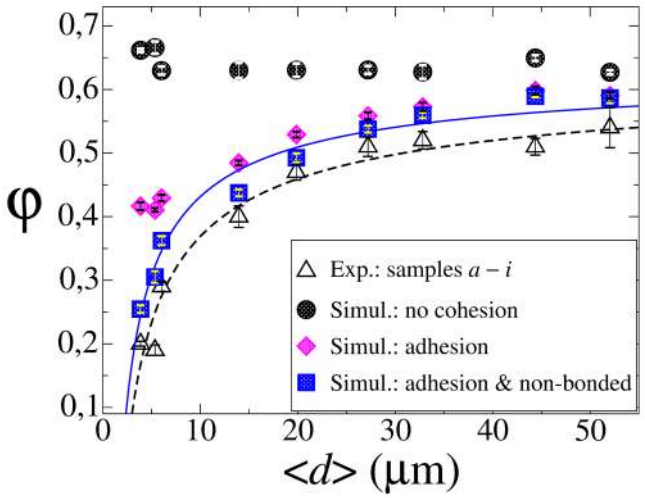

Figure 3 | Packing fraction as a function of the average particle size. Empty symbols show experimental results for samples *a–i*, each corresponding to a different particle size distribution, specified by Fig. 1 and Tab. I. Results of the simulation are shown by filled symbols: Circles: no attractive forces; diamonds: with adhesion (JKR model); squares: with both adhesion and non-bonded van der Waals interactions. The lines show the best fit to the data using Eq. (12).

$$A_H = 24\pi D_{\mathrm{min}}^2 \gamma. \tag{10}$$

Furthermore, D_{min} is a parameter introduced to avoid the singularity of the Hamaker equation at $\xi = 0$. As a matter of fact, the surface of the particles is not smooth, such that there is always a minimal distance D_{min} between the particles at contact[38,39]. Here we take the value $D_{\mathrm{min}} = 1.65\text{Å}$[2,39]. Finally, D_{max} is the maximal (cutoff) distance of the van der Waals interaction, which is set as 1 μm.

Results

For the simulation we adopt the mass fractions of each particle size in the sample as obtained from the corresponding volume density distribution used in the experiment, Fig. 1. Silica glass particles are deposited in a rectangular box of lateral dimensions $L_x \times L_y$, where $L_x = L_y = 12\langle d\rangle$, with $\langle d\rangle$ standing for the mean particle size, specific for each sample. We apply periodic boundary conditions in the directions x and y (Fig. 2). A frictional wall is placed at the floor, $z = 0$, while the height of the box (L_z) is set large enough such as to produce packings with depth larger than $30\langle d\rangle$. The equations used for computing the forces between particles and the frictional wall at the bottom are the same used for modeling particle-particle collisions where one of the contact partners is of infinite mass and radius. For particle-wall contacts we neglect attractive forces.

For initial conditions, we place the particles at random positions (initial space filling $\varphi(0) \approx 0.2$) such that the particles do not touch one another (Fig. 2a). At time $t = 0$ the particles are released from rest and are deposited at the bottom due to gravity. The density of the sediment, φ, was computed after full relaxation, indicated by vanishing kinetic energy of the particles, via

$$\varphi \equiv \frac{\sum_i \frac{4}{3}\pi R_i^3}{L_x L_y (H_u - H_l)}, \tag{11}$$

where the sum runs over all particles whose position is within the range $(H_l, H_u) = (0.3, 0.7)z_{\mathrm{max}}$ with z_{max} being the vertical position of the highest particle in the packing. We found that the value of φ obtained for a specific particle size distribution and inter-particle force model varies by a negligible amount over different realizations. Therefore, the values of φ presented in the following were obtained

by dividing both lateral dimensions of the box in two equal parts and averaging over the 4 resulting boxes, whereas the corresponding standard deviation associated with the different simulation data is indicated by the error bars in Fig. 3.

Figure 3 shows the packing fraction for the samples *a–i* as obtained in the experiment and the simulations. In the experiment, we find nearly constant packing fraction, φ, for samples *f–i* where $\langle d\rangle \gtrsim 25\,\mu$m (see Figs. 1f–i) while for smaller particles φ decreases rapidly. Such a behavior of increasing porosity with decreasing particle size was also noted in previous experiments, and has been attributed to the tendency of fine particles to form tree- or chain-like packing structures as well as large agglomerates[1].

In order to understand the effect of inter-particle forces on the packing properties and, thus, the dependence of the packing fraction on the average particle size, we performed three different groups of simulations, which are described below.

Pure viscoelastic interaction. In the first group of simulations, the packings are produced by neglecting attractive interaction forces, resulting in almost constant packing fraction (filled circles in Fig. 3) in disagreement with the experimental data. In fact we observe even a small (statistically not significant) increase of the packing fraction for small average particle size. This effect may be understood since the samples of smallest average size reveal the largest width of the distribution (Figs. 1a,b and Tab. I). Therefore, the small particles can efficiently fill the pores between the large ones, thus leading to lower porosity values. The effect of pore filling in polydisperse packings has been extensively studied in the past and provides the physical mechanism exploited in the search for the optimal packing of non-cohesive granular materials[15–20].

Adhesive viscoelastic interaction. In the second group of simulations, the adhesive force model (Eq. (6)) is incorporated leading to a decrease of the packing fraction for all samples and in particular for small particles (filled diamonds in Fig. 3). Obviously, for small particles, adhesion becomes dominant over gravity and, thus, particles tend to stick to one another leading to higher porosity, resulting in a decay of the packing fraction with decreasing particle size. While the decay follows the experimental data for $\langle d\rangle \gtrsim 20\,\mu$m, in agreement with earlier findings obtained for monosized particles[13], for smaller particles the data disagree due to increasing importance of van der Waals forces neglected here. Moreover, for all particle sizes, there is a significant offset between the experimental and numerical data.

Full model, including viscoelastic, adhesive, and van der Waals interaction. For the third group of simulations we applied the full model of particle interaction, that is Eqs. (6) and (9) (filled squares in Fig. 3). The resulting packing fraction agrees rather well with the experiment, as compared with the previous simulations where parts of the interaction force were neglected. In particular, for small particles, $\langle d\rangle \lesssim 20\,\mu$m, the packing fraction decreases rapidly, in agreement with the experiment. For larger $\langle d\rangle$, we obtain essentially the same packing density as found in simulations including only adhesive forces, since the ratio of van der Waals forces (which scale with R; cf. Eq. (9)) and particle weight (which scales with R^3) decreases as $1/R^2$. Therefore, the contribution of van der Waals forces renders negligible as the particle size increases. The full line in Fig. 3 shows the best fit of the function

$$\varphi = \varphi_\infty - \frac{C}{\langle d\rangle^\alpha}, \tag{12}$$

to the numerical data, where $\varphi_\infty \approx 0.64$ is the packing density in the limit of large particles, where attractive forces are negligible. In this limit the packing fraction approaches the value found for cohesionless particles (filled circles in Fig. 3). Table II shows the fit parameters, C and α, together with the corresponding values for the experimental data (dashed line in Fig. 3), being in good agreement.

Obviously, the function Eq. (12) cannot be universal as $\lim_{\langle d\rangle\to 0}\varphi \to -\infty$, however, for particle sizes in a certain range, $10^0 \lesssim \langle d\rangle/\mu\text{m} \lesssim 10^2$ it describes the packing fraction rather well. Indeed, we have showed, for the first time, that both experimental and numerical data of the packing fraction of fine powders as a function of the average particle size can be fitted by a surprisingly simple expression (Eq. (12)), which contains only 2 fit parameters. However, certainly Eq. (12) is not unique since the values of the fit parameters depend on material properties, in particular on the cohesion energy density, γ which was not investigated here.

Table II | Fit parameters of Eq. (12) for the experimental and numerical data and the corresponding correlation coefficient

	C	α	correlation coeff.
experiment	1.049	0.587	0.981
simulation	0.990	0.676	0.987

Discussion

We studied the packing fraction, φ, of fine glass powders of given particle size distribution by means of DEM simulations in comparison with experimental results. Three sets of simulation were performed, assuming different particle interaction forces.

For pure viscoelastic interaction (set I) we obtain packing fraction almost independently of the mean particle size, $\langle d\rangle$, with a slight tendency of increasing φ for small particles which may be explained by geometric effects (pore filling). This behavior, $\varphi \approx$ const., agrees with the experiment for large particle size, $\langle d\rangle \gtrsim 40\,\mu$m but disagrees for smaller particle size.

Simulations incorporating JKR-type adhesive forces (set II) reveal a clear decay of φ with decaying $\langle d\rangle$ and we obtain a good agreement with the experiment for $\langle d\rangle \gtrsim 20\,\mu$m while the data diverge for smaller particles.

The third set of simulation assumed inter-particle forces due to viscoelastic, JKR-adhesive and non-bonded van der Waals interaction (set III) which finally allowed to reproduce the experimentally found packing fraction for the full interval $4\,\mu\text{m} \lesssim \langle d\rangle \lesssim 52\,\mu$m.

Therefore, we conclude that for a predictive simulation of fine powder behavior, both adhesive and van der Waals forces are essential and should, thus, be considered in DEM simulations. Neglecting any of these contributions in simulation of fine powders may lead to unreliable results.

We believe that this result, obtained for the packing of fine glass powders will be of relevance also for other related systems[40], in particular, when the system contains a significant fraction of small particles or a wide distribution of particle sizes. The present study should be now continued by performing a detailed investigation of the different packing structures obtained in experiments and simulations using different material properties and particle size distributions. Such an investigation could be conducted by using e.g. scattering or tomography to directly compare spatial correlations between experimental and modelled particles and to shed further light on the role of polydispersity on the packing behavior of the powder system.

We note that other factors may further influence the exact value of the packing fraction. In particular, experimental spherical particles generally display small variations from the perfect spherical shape, which can affect local properties of the packing. In order to account for rolling resistance of slightly non-spherical particles, the DEM simulations of Ref. [41], which used a linearized version of Eq. (9), included an empiric model for rolling friction. However, Ref. [41] did not consider the contribution of adhesive forces predicted by the JKR theory (see Eq. (6)). Indeed, recent DEM simulations of packings of

monosized rods with adhesion forces modeled with the JKR theory[13] suggested that a slight degree of non-sphericity should cause negligible change in the solid fraction of the bulk. For spherical particles, rolling friction plays a minor role for particle motion compared to sliding friction[42]. Further, the effect of adhesion on the bulk solid fraction is predicted to be greater the larger the particles' aspect ratios[13]. To simulate powder particles of irregular shapes, our model should be thus extended in order to incorporate the multisphere method (see e.g. Refs. [10, 13, 43] and references therein), while accounting for both adhesion and non-bonded van der Waals forces between the particles as described in the present work.

Moreover, attractive forces due to the formation of liquid bridges between the particles[39] that have been neglected in the present simulations will also play an important role in the experiments since these were performed under ambient conditions in the laboratory at a relative humidity of around 40%. Indeed, the values of surface energy density and Hamaker constant used in the simulations are consistent with those applied in previous experiments under comparable experimental conditions[3]. However, while we have shown that a remarkable improvement in the quantitative agreement between numerical and experimental measurements of the solid fraction of fine polydisperse powders can be obtained by including adhesive and non-bonded van der Waals forces in DEM simulations, our study must be further improved in the future by inclusion of liquid bridges in the DEM simulation. This further extension of the DEM model certainly should further improve the quality of the agreement between numerical predictions and experimental results.

Experimental particles of different sizes may also have different friction coefficients, which may further affect the value of bulk packing fraction φ. However, the effect of μ on φ was shown in many previous DEM simulations to be negligibly small (less than 10%; see e.g. Refs. [44, 45]) compared to the strong dependence of φ on $\langle d \rangle$ found in our experiments (Fig. 3). Moreover, fluid friction on air is known to affect the deposition dynamics of fine particles[46,47], however, clearly the cohesive properties of such particles dominate the static behavior of the bulk. Furthermore, it is well known that the solid fraction of a granular system may be influenced by the assembly procedure[10,48]. Therefore, our expression for predicting the packing fraction of powders as a function of the average particle size, Eq. (12), should be tested not only for different size distributions and material properties but also for different assembly procedures. Indeed, the bulk solid fraction of granular systems made of non-cohesional spherical particles is close to 0.64 (the random close packing[49], consistent with our simulation results denoted by the black circles in Fig. 3), and is well reproducible by many different assembly procedures[50,51]. In contrast, numerical simulations[41,52] show that the packing behavior of cohesive powders under compression may strongly depend on the preparation method. However, the aim of our work is to reproduce the specific conditions of the experiments, in which the powder is deposited into a recipient and is not subject to compression (see for instance previous DEM simulations of Refs. [7, 11, 13, 16, 44, 45]). Therefore, on the basis of the exposed above, we conclude that attractive particle interaction forces play a major role for the bulk solid fraction of fine polydisperse powders made of spherical particles, while additionally including the aforementioned factors should further improve the quantitative assessment of the packing behavior of cohesive granular systems.

Methods

Experimental details. Commercially available, spherically-shaped glass particles SiLibeads Type S (0–20 μm, 0–50 μm, 40–70 μm, Sigmund Lindner GmbH) have been classified using a 50 ATP Turboplex air classifier (Hosokawa Alpine AG) to obtain glass powders of different particle size used in the experiment.

The particle size distributions of the samples *a–i* of glass powders have been obtained by laser diffraction particle sizing using a Mastersizer 2000/Hydro 2000S (Malvern). An aqueous suspension of the glass particles has been diluted as appropriate prior to measurement with deionized water. In each measurement, the respective scattering intensity raw data of the dispersed particles are collected by a detector array in dependency on the scattering angle and converted to particle size distributions by a Mie theory algorithm that is implemented in the Mastersizer 2000 software. As Mie scattering describes the scattering of electromagnetic radiation by a homogeneous sphere, reliable size distributions are obtained in the case of the almost transparent and spherical glass beads considered in this study. For evaluation a refractive index of 1.52 for the glass beads and 1.333 for water was used, respectively.

In order to determine the bulk density of packings we poured approx. 80 mL of the respective glass powder into a graduated cylinder using a funnel of a total nominal volume of 100 mL (resolution of 0.5 mL) and obtained the occupied volume from the filling height. The funnel has top and bottom diameters of 10 cm and 1.5 cm, respectively, and an angle of 60°, while the diameter of the cylinder is 3.5 cm. The experiments were performed with the funnel outlet at a constant height of about 12 cm from the recipient's bottom. For all samples, after the powder was poured from the funnel into the recipient, the measurements of the packing fraction were performed without applying any tapping or compression to the granular material. The bulk density was obtained by dividing the mass of the material as obtained using a lab balance (resolution 1 mg) by the occupied volume. The packing fraction, φ, is obtained by dividing the bulk density by the density of the solid. The results obtained for the packing fraction were found to vary only marginally over the 5 different experimental realizations (see standard deviation indicated by the error bars in Fig. 3).

Table III | Numerical values of the parameters used in the simulations

parameter	symbol	value
particle material density		2500 kg/m^3
Young's modulus	Y	63 GPa
Poisson's ratio	ν	0.24
Coulomb's friction coefficient	μ	0.50
surface energy density	γ	0.05 J/m^2
Hamaker constant	A_H	10^{-19} J

DEM. The integration was performed using LIGGGHTS[26] which was extended to account for the attractive particle interaction forces (Eqs. (6) and (9)). The Young modulus and particle mass density are taken from the data sheet of the material used in the experiments. For the surface energy density of the beads we use a value which is typical for SiO_2 and calculate the Hamaker constant using Eq. (10). Moreover, the Poisson's ratio of silica glass is used in the simulations (see e.g.[53]). For the friction coefficient μ we take a value that is typically used in simulations of granular materials (see e.g.[10]). The numerical values are given in Tab. III.

The integration time step Δt must be small enough to accurately solve Newton's equations for the particle interaction. For undamped, non-adhesive collisions ($A_n = \gamma = 0$), the duration T_{col} of the collision can be estimated using the equation[22],

$$T_{col} \approx 3.21 (M_{eff}/\rho)^{2/5} \cdot v_{imp}^{-1/5}, \tag{13}$$

where v_{imp} is the impact velocity. Typically a timestep smaller than about $T_{col}/50$ is recommended[54]. Thus, in order to determine the timestep, first we estimate, using Eq. (13), the collision time of the smallest particles in the particle size distribution using a reference impact velocity $v_{imp} = 1.0$ m/s (which is in fact an upper bound for the particle velocities observed in the simulations). Thereafter, we take Δt about 1/50 of T_{col}. For example, for the size distribution in Fig. 1i, the smallest value of particle diameter is $d \approx 20$ μm, for which we obtain $T_{col} \approx 62$ ns and thus we choose $\Delta t \approx 1.2 \times 10^{-9}$ s.

Solution of Eq. (8). In this Section, we present the expression which we use to obtain the contact radius $a(\xi)$. This contact radius is obtained by solving Eq. (8), which is a quartic equation in a of the form,

$$c_4 a^4 + c_3 a^3 + c_2 a^2 + c_1 a + c_0 = 0, \tag{14}$$

with $c_0 = R_{eff}^2 \xi^2$, $c_1 = -8(1-\nu^2)\pi\gamma R_{eff}^2 / Y$, $c_2 = -2R_{eff}\xi$, $c_3 = 0$ and $c_4 = 1$. The discriminant of Eq. (14) reads,

$$\begin{aligned}\Delta = {} & 256 c_4^3 c_0^3 - 192 c_4^2 c_3 c_1 c_0^2 - 128 c_4^2 c_2^2 c_0^2 + 144 c_4^2 c_2 c_1^2 c_0 \\ & - 27 c_4^2 c_1^4 + 144 c_4 c_3^2 c_2 c_0^2 - 6 c_4 c_3^2 c_1^2 c_0 - 80 c_4 c_3 c_2^2 c_1 c_0 \\ & + 18 c_4 c_3 c_2 c_1^3 + 16 c_4 c_2^4 c_0 - 4 c_4 c_2^3 c_1^2 - 27 c_3^4 c_0^2 \\ & + 18 c_3^3 c_2 c_1 c_0 - 4 c_3^3 c_1^3 - 4 c_3^2 c_2^3 c_0 + c_3^2 c_2^2 c_1^2,\end{aligned} \tag{15}$$

which becomes, by using the values of c_0, …, c_4 mentioned above,

$$\Delta = -4096 \left[\frac{\pi\gamma}{Y}\right]^2 R_{eff}^7 \xi^3 - 6912 \left[\frac{\pi\gamma}{Y}\right]^4 R_{eff}^8, \tag{16}$$

and is, thus, always negative. Therefore, Eq. (14) has 2 real roots and 2 imaginary roots. The solution $a(\xi)$ which corresponds to the contact radius of the JKR model is the one that is larger than $\sqrt{R_{eff}\xi}$ (the contact radius associated with the non-adhesive viscoelastic contact). Let us define the following quantities[55],

$$P = -\frac{c_2^2}{12} - c_0;$$
$$Q = -\frac{c_2^3}{108} + \frac{c_0 c_2}{3} - \frac{c_1^2}{8};$$
$$U = \left[-\frac{Q}{2} + \sqrt{\frac{Q^2}{4} + \frac{P^3}{27}} \right]^{1/3}; \quad (17)$$
$$s = \begin{cases} -5c_2/6 + U - \frac{P}{3U}, & \text{if } P \neq 0, \\ -5c_2/6 - Q^{1/3}, & \text{if } P = 0; \end{cases}$$
$$w = \sqrt{c_2 + 2s}, \quad \text{and} \quad \lambda = \frac{c_1}{2w}.$$

The real roots of Eq. (14) are

$$a_1 = \frac{1}{2} \cdot \left[w + \sqrt{w^2 - 4(c_2 + s + \lambda)} \right], \quad (18)$$

$$a_2 = \frac{1}{2} \cdot \left[w - \sqrt{w^2 - 4(c_2 + s + \lambda)} \right], \quad (19)$$

whereas the root that is larger than $\sqrt{R_{\text{eff}}\xi}$ is the root a_1. Therefore, the solution for the contact radius from Eq. (8) is $a(\xi) = a_1$, Eq. (18).

1. Yu, A. B., Bridgwater, J. & Burbidge, A. On the modelling of the packing of fine particles. *Powder Technol.* **92**, 185–194 (1997).
2. Götzinger, M. & Peukert, W. Dispersive forces of particle-surface interactions: direct AFM measurements and modelling. *Powder Technol.* **130**, 102–109 (2003).
3. Götzinger, M. & Peukert, W. Particle Adhesion Force Distributions on Rough Surfaces. *Langmuir* **20**, 5298–5303 (2004).
4. Castellanos, A. The relationship between attractive interparticle forces and bulk behaviour in dry and uncharged fine powders. *Adv. Phys.* **54**, 263–376 (2005).
5. Li, Q., Rudolph, V. & Peukert, W. London-van der Waals adhesiveness of rough-surfaced particles. *Powder Technol.* **161**, 248–255 (2006).
6. Severson, B. L., Keer, L. M., Ottino, J. M. & Snurr, R. Q. Mechanical damping using adhesive micro or nano powders. *Powder Technol.* **191**, 143–148 (2009).
7. Yang, R. Y., Zou, R. P. & Yu, A. B. Effect of material properties on the packing of fine particles. *J. Appl. Phys.* **94**, 3025–3034 (2003).
8. Dou, X., Mao, Y. & Zhang, Y. Effects of Contact Force Model and Size Distribution on Microsized Granular Packing. *ASME J. Manuf. Sci. Eng.* **136**, 021003 (2014).
9. Cundall, P. A. & Strack, O. D. L. A discrete numerical model for granular assemblies. *Geotechnique* **29**, 47–65 (1979).
10. Pöschel, T. & Schwager, T. *Computational Granular Dynamics* (Springer, Heidelberg, 2005).
11. Yang, R. Y., Zou, R. P. & Yu, A. B. Computer simulation of the packing of fine particles. *Phys. Rev. E* **62**, 3900–3908 (2000).
12. Yang, R. Y., Dong, K., Zou, R., Yu, A. B. & Guo, J. Packing of fine particles in an electric field. *Granul. Matter* **15**, 467–476 (2013).
13. Deng, X. L. & Davé, R. N. Dynamic simulation of particle packing influenced by size, aspect ratio and surface energy. *Granul. Matter* **15**, 401–415 (2013).
14. Deng, X. L., Scicolone, J. V. & Davé, R. N. Discrete element method simulation of cohesive particles mixing under magnetically assisted impaction. *Powder Technol.* **243**, 96–109 (2013).
15. Fuller, W. B. & Thompson, S. E. The laws of proportioning concrete. *Trans. Am. Soc. Civ. Eng.* **59**, 67–143 (1907).
16. Yi, L. Y., Dong, K. J., Zou, R. P. & Yu, A. B. Coordination Number of the Packing of Ternary Mixtures of Spheres: DEM Simulation versus Measurements. *Ind. Eng. Chem. Res.* **330**, 8773–8785 (2011).
17. Dias, R. P., Teixeira, J. A., Mota, M. G. & Yelshin, A. I. Particulate Binary Mixtures: Dependence of Packing Porosity on Particle Size Ratio. *Ind. Eng. Chem. Res.* **43**, 7912–7919 (2004).
18. Hopkins, A. B., Stillinger, F. H. & Torquato, S. Densest binary sphere packings. *Phys. Rev. E* **85**, 021130 (2012).
19. Reis, S. D. S., Araújo, N. A. M., Andrade Jr, J. S. & Herrmann, H. J. How dense can one pack spheres of arbitrary size distribution? *Europhys. Lett.* **97**, 18004 (2012).
20. Brouwers, H. J. H. Random packing fraction of bimodal spheres: An analytical expression. *Phys. Rev. E* **87**, 032202 (2013).
21. Johnson, K. L., Kendall, K. & Roberts, A. D. Surface energy and the contact of elastic solids. *Proc. R. Soc. Lond. Ser. A Math. Phys. Sci.* **324**, 301–313 (1971).
22. Schäfer, J., Dippel, S. & Wolf, D. E. Force Schemes in Simulations of Granular Materials. *J. Phys. I France* **6**, 5–20 (1996).
23. Kruggel-Emden, H., Simsek, E., Rickelt, S., Wirtz, S. & Scherer, V. Review and extension of normal force models for the Discrete Element Method. *Powder Technol.* **171**, 157–173 (2007).
24. Kruggel-Emden, H., Wirtz, S. & Scherer, V. A study on tangential force laws applicable to the discrete element method (DEM) for materials with viscoelastic or plastic behavior. *Chem. Eng. Sci.* **63**, 1523–1541 (2008).
25. Brilliantov, N. V., Spahn, F., Hertzsch, J.-M. & Pöschel, T. A model for collision in granular gases. *Phys. Rev. E* **53**, 5382–5392 (1996).
26. Kloss, C., Goniva, C., Hager, A., Amberger, S. & Pirker, S. Models, algorithms and validation for opensource DEM and CFD-DEM. *Prog. Comput. Fluid Dy.* **12**, 140–152 (2012); DCS Computing GmbH, *CFDEM - Open Source CFD, DEM and CFD-DEM*, http://www.cfdem.com/liggghts. Date of access: 23/05/2014.
27. Schwager, T. & Pöschel, T. Coefficient of restitution for viscoelastic spheres: The effect of delayed recovery. *Phys. Rev. E* **78**, 051304 (2008).
28. Schwager, T. & Pöschel, T. Coefficient of restitution of viscous particles and cooling rate of granular gases. *Phys. Rev. E* **57**, 650–654 (1998).
29. Ramírez, R., Pöschel, T., Brilliantov, N. V. & Schwager, T. Coefficient of restitution of colliding viscoelastic spheres. *Phys. Rev. E* **60**, 4465–4472 (1999).
30. Müller, P. & Pöschel, T. Collision of viscoelastic sphere: Compact expressions for the coefficient of normal restitution. *Phys. Rev. E* **84**, 021302 (2011).
31. Schwager, T., Becker, V. & Pöschel, T. Coefficient of tangential restitution for viscoelastic spheres. *Eur. Phys. J. E* **27**, 107–114 (2008).
32. Rycroft, C. H., Orpe, A. V. & Kudrolli, A. Physical test of a particle simulation model in a sheared granular system. *Phys. Rev. E* **80**, 031035 (2009).
33. Brilliantov, N. V., Albers, N., Spahn, F. & Pöschel, T. Collision dynamics of granular particles with adhesion. *Phys. Rev. E* **76**, 051302 (2007).
34. Barthel, E. Adhesive elastic contacts: JKR and more. *J. Phys. D.: Appl. Phys.* **41**, 163001 (2008).
35. Salmang, H. & Scholze, H. *Keramik* (Springer, Heidelberg, 2007).
36. Hamaker, H. C. The London-van der Waals Attraction Between Spherical Particles. *Physica* **4**, 1058–1072 (1937).
37. Eggersdorfer, M. L., Kadau, D., Herrmann, H. J. & Pratsinis, S. E. Fragmentation and restructuring of soft-agglomerates under shear. *J. Colloid Interface Sci.* **342**, 261–268 (2010).
38. Krupp, H. Particle Adhesion: Theory and Experiment. *Adv. Colloid Interface Sci.* **1**, 111–239 (1967).
39. Israelachvili, J. *Intermolecular & Surface Forces* (Academic Press, London, 1998).
40. Wu, C.-Y. & Pöschel, T. Micro-mechanics and dynamics of cohesive particle systems. *Granul. Matter* **15**, 389–390 (2013).
41. Gilabert, F. A., Roux, J.-N. & Castellanos, A. Computer simulation of model cohesive powders: Influence of assembling procedure and contact laws on low consolidation states. *Phys. Rev. E* **75**, 011303 (2007).
42. Pöschel, T., Schwager, T. & Brilliantov, N. V. Rolling friction of a hard cylinder on a viscous plane. *Eur. Phys. J. B* **10**, 169–174 (1999).
43. Parteli, E. J. R. DEM simulation of particles of complex shapes using the multisphere method: Application for additive manufacturing. *AIP Conf. Proc.* **1542**, 185–188 (2013).
44. Rosato, A. D., Dybenko, O., Horntrop, D. J., Ratnaswamy, V. & Kondic, L. Microstructure evolution in density relaxation by tapping. *Phys. Rev. E* **81**, 061301 (2010).
45. Silbert, L. E., Ertas, D., Grest, G. S., Halsey, T. C. & Levine, D. Geometry of frictionless and frictional sphere packings. *Phys. Rev. E* **65**, 031304 (2002).
46. Guo, Y., Wu, C.-Y. & Thornton, C. The effects of air and particle density difference on segregation of powder mixtures during die filling. *Chem. Eng. Sci.* **66**, 661–673 (2011).
47. Hilton, J. E. & Cleary, P. W. Granular flow during hopper discharge. *Phys. Rev. E* **84**, 011307 (2011).
48. Radjai, F. & Dubois, F. *Discrete Numerical Modeling of Granular Materials* (Wiley-VCH, Weinheim, 2011).
49. Baule, A., Mari, R., Bo, L., Portal, L. & Makse, H. A. Mean-field theory of random close packings of axisymmetric particles. *Nat. Commun.* **4**, 2194 (2013).
50. Aste, T., Saadatfar, M. & Senden, T. J. Geometrical structure of disordered sphere packings. *Phys. Rev. E* **71**, 061302 (2005).
51. Kamien, R. D. & Liu, A. J. Why is Random Close Packing Reproducible? *Phys. Rev. Lett.* **99**, 155501 (2007).
52. Strege, S., Weuster, A., Zetzener, H., Brendel, L., Kwade, A. & Wolf, D. E. Approach to structural anisotropy in compacted cohesive powder. *Granul. Matter*, doi:10.1007/s10035-013-0454-4 (2014).
53. Fan, L.-S. & Zhu, C. *Principles of Gas-Solid Flow* (Cambridge University Press, Cambridge, 1998).
54. Silbert, L. E., Ertaş, D., Grest, G. S., Halsey, T. C., Levine, D. & Plimpton, S. J. Granular flow down an inclined plane: Bagnold scaling and rheology. *Phys. Rev. E* **64**, 051302 (2001).
55. *Quartische Gleichung*, http://de.wikipedia.org/wiki/Quartische_Gleichung (Wikipedia). Date of access: 03/02/2014.

Acknowledgments

We thank Andreas Aigner and Nina Gunkelmann for discussion. The German Research Foundation (DFG) is acknowledged for funding through the Cluster of Excellence "Engineering of Advanced Materials" and the Collaborative Research Center SFB814 (Additive Manufacturing). The authors gratefully acknowledge the computing time granted by the John von Neumann Institute for Computing (NIC) and provided on the supercomputer JUROPA at Jülich Supercomputing Centre (JSC). We acknowledge support

by Deutsche Forschungsgemeinschaft and Friedrich-Alexander-Universität Erlangen-Nürnberg within the funding programme Open Access Publishing.

Author contributions

E.J.R.P. performed the numerical simulations and wrote the paper with T.P. J.S. and C.B. performed the experiments. J.S., K.W. and W.P. discussed the results with E.J.R.P. and T.P. and added content to the manuscript.

Additional information

Competing financial interests: The authors declare no competing financial interests.

How to cite this article: Parteli, E.J.R. *et al.* Attractive particle interaction forces and packing density of fine glass powders. *Sci. Rep.* **4**, 6227; DOI:10.1038/srep06227 (2014).